Soft Matter

COMMUNICATION

View Article Online
View Journal | View Issue

Cite this: *Soft Matter*, 2015, **11**, 1658

Unusual diffusing regimes caused by different adsorbing surfaces

Veridiana G. Guimarães,[a] Haroldo V. Ribeiro,[ab] Quan Li,[c] Luiz R. Evangelista,[a] Ervin K. Lenzi[ad] and Rafael S. Zola*[ab]

Received 19th January 2015
Accepted 23rd January 2015

DOI: 10.1039/c5sm00151j

www.rsc.org/softmatter

A confined liquid with dispersed neutral particles is theoretically studied when the limiting surfaces present different dynamics for the adsorption–desorption phenomena. The investigation considers different non-singular kernels in the kinetic equations at the walls, where the suitable choice of the kernel can account for the relative importance of physisorption or chemisorption. We find that even a small difference in the adsorption–desorption rate of one surface (relative to the other) can drastically affect the behavior of the whole system. The surface and bulk densities and the dispersion are calculated when several scenarios are considered and anomalous-like behaviors are found. The approach described here is closely related to experimental situations, and can be applied in several contexts such as dielectric relaxation, diffusion-controlled relaxation in liquids, liquid crystals, and amorphous polymers.

1. Introduction

Diffusion in confined geometries is present in several systems of interest, from impedance spectroscopy to living cells.[1–3] In many cases, one studies the diffusion time to probe geometry in porous media,[4,5] memory effects[6] and contributions of both.[7] It is very reasonable to consider that, in any confined system, the limiting surfaces may present the adsorption–desorption phenomena which greatly affect the dynamics of the diffusing species.[8] In fact, several processed products go through conversion by heterogeneous catalysis and chemical separation, often due to selective adsorption. In soft matter systems, diffusion and adsorption play very important roles. In liquid crystals, for example, the phenomena has been investigated in connection with anchoring energy,[9] surface transitions induced by adsorbed dyes controlled by light[10] and in association with the degradation of display performance due to adsorption of ions.[11] Polymers in solution may also be adsorbed onto surfaces, with a great deal of importance in pharmaceutical applications,[12] biophysics[13] and nanocomposite materials.[14] Diffusion and adsorption at the liquid–liquid interface has also been highly explored in the past few years in connection with nano-fabrication, biological systems,[15] colloids[16,17] and biosensing.[18]

In the literature, it has been investigated how confinement can lead to different diffusive regimes, leading, in certain cases, to anomalous-like diffusion. This has been explored, for example, when particles diffuse through membranes, zeolites[19] or in geometries with dead-ends.[20–22] Recently, a new approach for probing the type of anomalous diffusion has been introduced by particle tracking.[23] In particular, in ref. 24, a tracer diffusing in the space between the excluded volume obstacle systems was studied. It was shown that the tracer-obstacle adsorption and binding triggers a transient anomalous diffusion. Nonetheless, the role of adsorption on non-usual diffusive regimes and its applications are still limited, since many physical–chemical systems present very complex behaviors. In fact, confined systems subjected to adsorption–desorption have direct applications but have not been fully explored. Often the adsorption phenomena are treated theoretically by considering kinetic equations for each adsorbing surface. In ref. 25, a kinetic equation coupled with the diffusion equation was used considering different characteristic times. In ref. 26, the time dependency of the diffusion coefficient was explored when adsorption–desorption is considered. Nevertheless, in all cases only one mechanism for the adsorption–desorption phenomena was analyzed. In ref. 27, a non-singular kernel was used in the kinetic equation where depending on the chosen kernel, a different mechanism for the adsorption–desorption process is relevant. For simplicity, usually one assumes that the

[a]*Departamento de Física, Universidade Estadual de Maringá, Avenida Colombo 5790, 87020-900 Maringá, Paraná, Brazil. E-mail: rzola@utfpr.edu.br*

[b]*Departamento de Física, Universidade Tecnologica Federal do Paraná, Rua Marclio Dias 635, 86812-460 Apucarana, Paraná, Brazil*

[c]*Liquid Crystal Institute and Chemical Physics Interdisciplinary Program, Kent State University, Kent, OH 44242, USA*

[d]*Departamento de Física, Universidade Estadual de Ponta Grossa - Ponta Grossa, PR 87030-900, Brazil*

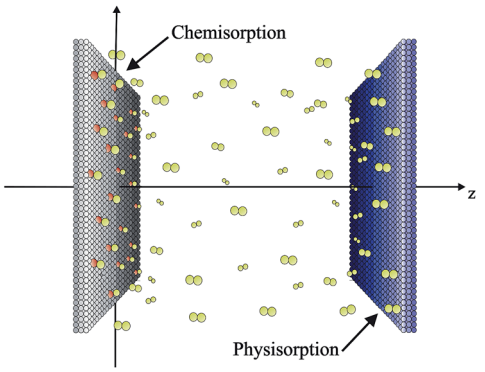

Fig. 1 Schematic representation of the system studied here. The diffusing species are represented by green dots. The left surface can chemically bond the particles (chemisorption, shown by the red dot) and the right surface adsorbs through physisorption.

kinetics at both surfaces are the same, including adsorption–desorption times and the mechanism involved (*i.e.* chemisorption or physisorption). This implies that the dynamics at both surfaces are the same, resulting in an even distribution of particles across the cell which leads to a monotonic behavior of the diffusion coefficient with time.[26]

Here, we obtain the exact solution for the time evolution of bulk and surface particles when the surfaces are non-identical, presenting also different mechanisms and time evolution in the adsorption–desorption phenomena. Such model has a direct application in fuel cells (hybrid microfluidic fuel cells, for example), where electrode materials may present different materials and thus different adsorption kinetics.[28] Furthermore, it finds applications in liquid crystals doped with dyes, hybrid aligned liquid crystal cells,[29] liquid crystal wetting layers[30] and polymer adsorption in confined geometries.[31] All of these systems may present different boundaries in confined geometries which allows direct application of our model. In general, our model may find application in any system where more than one adsorbing surface is present, since in real experimental situations it is difficult to make two surfaces behave exactly the same way.

In this article, the dynamics of a confined liquid with dispersed neutral particles is studied. It is shown that the kinetics at one surface can greatly affect the dynamics at the other surface and consequently, the whole system. The temporal behavior of the surface densities $\sigma(t)$ and the bulk density $\rho(z, t)$ is calculated by solving the diffusion equation coupled with kinetic equations at the walls when both surfaces present chemisorption (but with different kinetics) and when one surface adsorbs chemically and the other surface presents physisorption. Fig. 1 shows a schematic illustration of the system studied here. The dispersion of the system is analyzed via bulk distribution and anomalous-like behaviors are found depending on the choice of the parameter characterizing the walls.

2. Models

We consider a sample in the shape of a slab containing an isotropic fluid with neutral particles. It is assumed that the only direction relevant to the particle diffusion is z, being the limiting surfaces located at $z = 0$ and $z = d$. The bulk density $\rho(z, t)$ is governed by the diffusion equation

$$\frac{\partial \rho}{\partial t} = D\frac{\partial^2 \rho}{\partial z^2}, \tag{1}$$

where D is the medium diffusion coefficient. The surface densities at $z = 0$ and $z = d$ are denoted by σ_0 and σ_d, respectively. The kinetic equations governing the boundaries are[27,32]

$$\frac{\mathrm{d}\sigma_0}{\mathrm{d}t} = \kappa_0 \rho(0, t) - \int_0^t S_0(t - t')\sigma_0(t')\mathrm{d}t', \tag{2}$$

$$\frac{\mathrm{d}\sigma_d}{\mathrm{d}t} = \kappa_d \rho(d, t) - \int_0^t S_d(t - t')\sigma_d(t')\mathrm{d}t', \tag{3}$$

where κ_i with $i = 0, d$ is a parameter connected to the adsorption phenomena, being related to the a characteristic adsorption time $\tau_{\kappa_i} = d/2\kappa_i$ and $S_i(t)$ $(i = 0, d)$ is a kernel that governs the adsorption–desorption phenomena depending on the choice of the function. Eqn (2) and (3) state that the time variation of the surface density of adsorbed particles depends on the bulk density of particles just in front of the adsorbing surface, and on the surface density of particles already adsorbed. In fact, it is possible to connect the phenomenological eqn (2) and (3) with microscopic parameters representing the van der Waals interaction between the particles and the surfaces.[25] It is a balance equation first introduced without the kernel notation[32] (*i.e.*, $\mathrm{d}\sigma(t)/\mathrm{d}t = \kappa\rho(z, t) - 1/\tau\sigma(t)$). The presence of the kernel, introduced in ref. 27, dictates the nature of the adsorption phenomena. A kernel like $S_i(t)$ has been used in several contexts to express non-Debye relaxation,[33,34] yielding non-trivial behavior description and allowing different or combined effects in a single kinetic equation.[27] In this work, two kinetic equations, one for each surface, are used and the presence of the kernel is connected to the specific dynamics of the system. It states that the time to adsorb a particle may depend on the previous state of the particle, adding thus short or long-range memory effects that can be related, for example, to the energy loss during the collision with the surface in a previous adsorption–desorption process. Since the bulk density of particles is allowed to fluctuate, $\sigma_0 + \sigma_d + \int_0^d \rho(z, t)\mathrm{d}z = \rho_0 d$, where $\rho(z, 0) = \rho_0$. In what follows, the Laplace transform method can be applied to solve eqn (1), so

$$\rho(z, s) = \frac{\rho_0}{s} + A(s)\sinh\left(\sqrt{s/D}z\right) + B(s)\cosh\left(\sqrt{s/D}z\right), \tag{4}$$

where $\rho(z, s) = \int_0^\infty \rho(z, t)\mathrm{e}^{-st}\mathrm{d}t = \mathscr{L}\{\rho(z, t)\}$. Furthermore, from eqn (2) and (3), we obtain

$$sG_0(s) - \sigma_0(0) = \kappa_0\rho(0, s) - S_0(s)G_0(s),$$

$$sG_d(s) - \sigma_d(0) = \kappa_d\rho(d, s) - S_d(s)G_d(s), \tag{5}$$

where $G_i(s) = \mathscr{L}\{\sigma_i(t)\}$ and we assume that $\sigma_i(0) = 0$. By combining eqn (4) and (5) with the conditions on the current

density $j(i, t) = d\sigma_i/dt$, the parameters $A(s)$ and $B(s)$ are found. It is possible to show that, in Laplace's space, the surface densities are given by

$$G_i(s) = \frac{\kappa_i\rho_0\left[C_1(s)\sinh\left(d\sqrt{\frac{s}{D}}\right) + \kappa_j s\cosh\left(d\sqrt{\frac{s}{D}}\right) - \kappa_j s\right]}{s\left\{\sqrt{\frac{s}{D}}\sinh\left(d\sqrt{\frac{s}{D}}\right)C_2(s) + s\cosh\left(d\sqrt{\frac{s}{D}}\right)C_3(s)\right\}}, \quad (6)$$

with

$$C_1(s) = \sqrt{sD}\left(S_j(s) + s\right),$$

$$C_2(s) = D(S_0(s) + s)(S_d(s) + s) + \kappa_0\kappa_d s,$$

$$C_3(s) = \kappa_d(S_0(s) + s) + \kappa_0(S_d(s) + s),$$

where $j = 0$, when $i = d$, and $j = d$, when $i = 0$. Eqn (6) shows that the densities of particles at one surface depend on the dynamics of adsorption–desorption that is happening on the other surface. In order to obtain the solutions $\sigma_i(t)$, the inverse Laplace transform of eqn (6) must be calculated. This can be done only when $S_i(t)$ is given.

3. Results and discussion

We first address the case where both surfaces present a pure chemisorption process, however, each surface has its own adsorption and desorption times, which means $S_i(t) = \delta(t/\tau_i)/\tau_i^2$ where τ_i is a parameter connected to the desorption time. In this case, we are assuming that the molecule on the surface has lost the memory of the preceding state. For this reason, the kernel is a localized function of time.[27,35] Now, the inversion can be performed with Browinch's integral in the complex plane with the residue technique.[36] The residue is calculated at each pole, which means finding the zeros in the denominator of eqn (6) (see Appendix A for details). This denominator has a zero in $s = 0$ and the periodic poles (zeros) are given by

$$\tan[X_n] = \frac{\tau_D X_n\left[4\tau_0\tau_d X_n^2\left(\tau_{\kappa_0} + \tau_{\kappa_d}\right) - \tau_D\left(\tau_0\tau_{\kappa_d} + \tau_d\tau_{\kappa_0}\right)\right]}{\tau_D^2\tau_{\kappa_0}\tau_{\kappa_d} + 16\tau_0\tau_d\tau_{\kappa_0}\tau_{\kappa_d}X_n^4 - \tau_D X_n^2\left[\tau_0\tau_d\tau_D + 4\tau_{\kappa_0}\tau_{\kappa_d}(\tau_0 + \tau_d)\right]}, \quad (7)$$

where $\tau_D = d^2/D$ (the diffusion time), $\tau_{\kappa_i} = d/2\kappa_i$ (the adsorption time) and X_n refers to the roots of eqn (7). The solution of eqn (6) can thus be written as a series expansion when the residue in $s = 0$ and in $s = X_n$ (n = integer) are calculated. This series yields two equations for $\sigma_i(t)$ (see Appendix A) and have been manipulated by means of the software Mathematica 9.0.

The temporal behaviors of $\sigma_0(t)$ and $\sigma_d(t)$ (eqn (17) and (18), respectively) are shown in Fig. 2. The parameters used for this and for the next plots were found in the literature where a kinetic equation similar to the one used here has been employed to some systems of interest.[34] In fact, some of these parameters can be estimated for a typical liquid sample. It has been found that the desorption parameter τ ranges from 0.01 s in liquid crystal samples to 1 s in some isotropic liquids by means of comparing

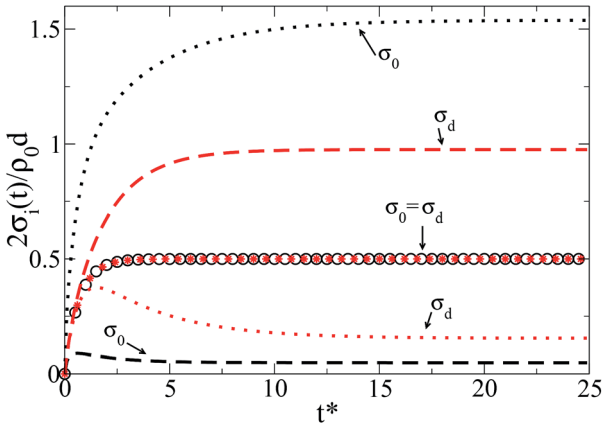

Fig. 2 Temporal behavior of $\sigma_0(t)$ and $\sigma_d(t)$ *vs.* $t^* = 4t/\tau_D$ when both surfaces have the same adsorbing mechanism ($S_i(s) = 1/\tau_i$ but the characteristic times are different). The solid and empty circles represent the case where $\tau_d/\tau_0 = \tau_{\kappa_0}/\tau_0 = \tau_{\kappa_d}/\tau_0 = 1$ and $\tau_D/\tau_0 = 4$. The dotted curves show the case where $\tau_d/\tau_0 = \tau_{\kappa_d}/\tau_0 = 1$, $\tau_D/\tau_0 = 4$, and $\tau_{\kappa_0}/\tau_0 = 0.1$. The dashed curves represent the case where $\tau_d/\tau_0 = 20$, $\tau_D/\tau_0 = 40$ and $\tau_{\kappa_0}/\tau_0 = \tau_{\kappa_d}/\tau_0 = 10$.

the theory with experimental data. Similarly, the adsorption parameter κ usually is in the order of $\sim 10^{-6}$ m s^{-1}.[25,32–34,37] From this value, one can estimate τ_κ for a typical 10 μm cell as being $\tau_\kappa \approx 5$ s. The parameter τ_D, for the same kind of cell can be calculated by using a typical diffusion coefficient $D \approx \times 10^{-11}$ m^2 s^{-1}, so $\tau_D \approx 10$ s. For the following figures, we scaled all the parameters with respect to τ_0 and changed the values of the parameters in order to highlight the effect of each parameter within the values previously discussed. In Fig. 2, for the case where the parameters are the same (identical surfaces), shown by the open and closed circles, the densities are the same and equal to the result presented in ref. 25. It is interesting to note how the dynamics on one surface can directly affect the other. In Fig. 2, for the dotted curves, the adsorption time of the surface located in $z = 0$ is much shorter than the adsorption time of the opposite surface ($\tau_{\kappa_d}/\tau_0 = 1$ while $\tau_{\kappa_0}/\tau_0 = 0.1$). This causes σ_0 to increase very rapidly in the initial moments. Since there is a higher drift current towards this surface, the particles in the bulk migrate towards the surface located in $z = 0$. The wall in $z = d$ (σ_d) thus adsorbs in the initial moments, then desorbs some of its particles until the system reaches equilibrium. In Fig. 2, the dashed curve shows the case where both surfaces have the same adsorption time. Nonetheless, the desorption time of σ_0 is much shorter than σ_d. This causes σ_0 to reach a smaller density value when the system reaches equilibrium, since it desorbs faster than the other surface.

From eqn (4), $\rho(z, t)$ can be obtained. Eqn (6) has the same poles as eqn (4) and therefore eqn (7) is also used in the calculation of $\rho(z, t)$ (see Appendix A). Fig. 3 shows the bulk distribution at several times for the same parameters of Fig. 2 (dotted). The difference in the parameters at each surface breaks the even symmetry expected for the particle distribution.

Next, the case where each surface has a different mechanism is explored. We make $S_0(t) = \delta(t/\tau_0)/\tau_0^2$ and

$$S_d(t) = 1/(\tau_d\tau_a)e^{-t/\tau_a}, \quad (8)$$

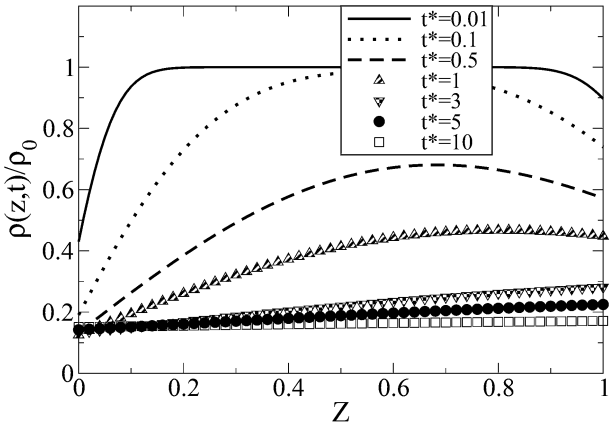

Fig. 3 Normalized bulk density *vs.* $Z = z/d$ for several values of t^*. The curves were calculated for $\tau_d/\tau_0 = \tau_{\kappa_d}/\tau_0 = 4$, $\tau_D/\tau_0 = 4$, and $\tau_{\kappa_0}/\tau_0 = 0.1$.

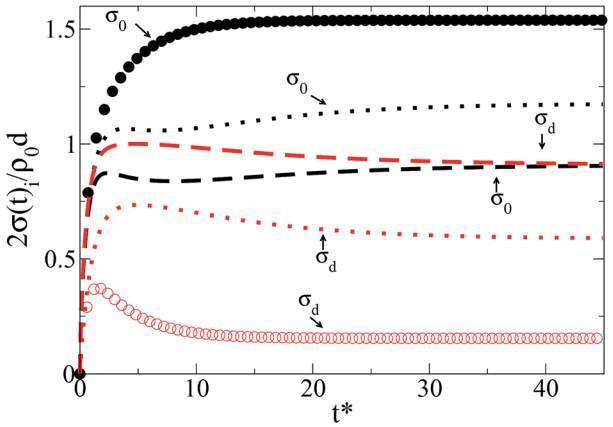

Fig. 4 Temporal behavior of $\sigma_0(t)$ and $\sigma_d(t)$ *vs.* $t^* = 4t/\tau_D$ when $S_0(s) = 1/\tau_0$ and $S_d(s) = 1/[(s + 1/\tau_a)\tau_d\tau_a]$. The closed and open circles represent the case where $\tau_D/\tau_0 = 4$, $\tau_d/\tau_0 = \tau_{\kappa_d}/\tau_0 = 1$, $\tau_{\kappa_0}/\tau_0 = 0.1$ and $\tau_a/\tau_0 = 0.1$. The dotted curves show the case where $\tau_D/\tau_0 = 5$, $\tau_d/\tau_0 = 5$, $\tau_{\kappa_d}/\tau_0 = 1$, $\tau_{\kappa 0}/\tau_0 = 0.1$, and $\tau_a/\tau_0 = 3.5$. The dashed curves represent the case where $\tau_D/\tau_0 = 5$, $\tau_d/\tau_0 = 1$, $\tau_{\kappa_d}/\tau_0 = \tau_{\kappa_0}/\tau_0 = 0.1$, and $\tau_\alpha/\tau_0 = 3.5$.

where τ_a is a characteristic time. Usually, a kernel like the one in eqn (8) is used to describe "memory", as it is done in the theory of dielectrics, in which the relaxation depends on the previous state. It has also been used in the context of adsorption–desorption to describe the memory of the system. This kernel incorporates a memory effect in the adsorption–desorption phenomena by assuming that during a time τ_a the particle being adsorbed retains knowledge of its preceding state. To account for this phenomenon, the proposed kernel has a nonzero width in time, *i.e.*, it introduces a time delay in the desorption rate. The physical reasons for this behavior can be understood as follows: the molecules in the bulk have an amount of energy, so that, when they are adsorbed in the wells at the surface, the energy is still rather large and, for this reason, they are desorbed soon loosing part of the energy. This phenomenon continues until the energy lost from the particle is such that the steady state is reached, after a characteristic time τ_a. Thus, the system studied now can be interpreted as having one surface treated to present chemisorption and the opposite surface treated to present physisorption. Replacing $S_0(t)$ and $S_d(t)$ into eqn (6) allows the calculation of the temporal densities of adsorbed and bulk particles, which is done by the same procedure mentioned earlier. Both the surface and bulk densities are written as a series expansion after performing the Laplace inversion, whose eigenvalues are the roots given by eqn (9). With both densities in hands, all the relevant quantities to the problem can be calculated. The temporal behavior of σ_0 and σ_d for several values of the parameters are shown in Fig. 4. The pair of open and closed circles represent the density at $z = 0$ and $z = d$, respectively, when $\tau_D/\tau_0 = 4$, $\tau_d/\tau_0 = \tau_{\kappa_d}/\tau_0 = 1$, $\tau_{\kappa_0}/\tau_0 = 0.1$ and $\tau_a/\tau_0 = 0.1$. Notice that in this case, since the memory parameter τ_a is small, we recover the behavior shown by the dotted curve in Fig. 1, where both surfaces are represented by delta functions. The other two pairs (dotted and dashed curves) accounts for long τ_a, thus, for a pronounced memory effect at the surface located at $z = d$. Nonetheless, the non-monotonic behavior is observed for both surfaces, depending also on the parameters τ_{κ_i} and τ_i. For the dotted curve, the adsorption time of $\sigma_0(t)$ is shorter than the one on the other surface. This causes $\sigma_0(t)$ to grow fast, but it oscillates due to the memory term and the long desorption time in $\sigma_d(t)$. For the dashed curve, both surfaces have the same adsorption and desorption times. As a consequence, both surfaces reach the same density after a long period of time, caused by the non-Markovian behavior of the adsorption process occurring at $z = d$. The long time to reach the same density is therefore associated with the memory in the adsorption–desorption process, affecting both surfaces.

$$\tan[X] = \frac{T_1 + \tau_D\left(\tau_0\tau_{\kappa_d} + \tau_d\tau_{\kappa_0}\right) - 4\tau_d X^2\left(\tau_0\left(\tau_{\kappa_0} + \tau_{\kappa_d}\right) + \tau_a\tau_{\kappa_0}\right)}{T_2 + \tau_0\tau_d X\left(\tau_D - 4\tau_a X^2\right)} \tag{9}$$

where

$$T_1 = \frac{16\tau_0\tau_a\tau_d X^4\left(\tau_{\kappa_0} + \tau_{\kappa_d}\right)}{\tau_D},$$

$$T_2 = \frac{\tau_{\kappa_0}\tau_{\kappa_d}(4\tau_0 X^2 - \tau_D)\left({\tau_D}^2 + 16\tau_a\tau_d X^4 - 4\tau_d\tau_D X^2\right)}{{\tau_D}^2 X}.$$

The behavior of $\rho(z, t)/\rho_0$ *vs.* $Z = z/d$ for several $t^* = 4t/\tau_D$ when $S_0(s) = 1/\tau_0$ and $S_d(s) = 1/[(s + 1/\tau_a)\tau_d\tau_a]$ is given in Fig. 5. Notice the large variation of the bulk density as the surfaces adsorb (desorb). These plots correspond to the dashed curves in Fig. 4. Interestingly, the bulk density saturates with a larger amount of particles than it had for certain previous times, for example, for $t^* = 40$ compared to $t^* = 5$. This behavior is caused by the long time for the surface located at $z = d$ to desorb the initially adsorbed particles (dashed curve, Fig. 4).

Next, by using the solution of eqn (5), the variance of $z(\Delta z)^2 = \langle(z - \langle z\rangle)^2\rangle$ is calculated. Here, $\langle\ldots\rangle$ refers to ensemble average. It is an important parameter because it is a measure of the spread of the distribution about its average value, used to characterize the time dependent diffusion coefficient[26] ($D(t) =$

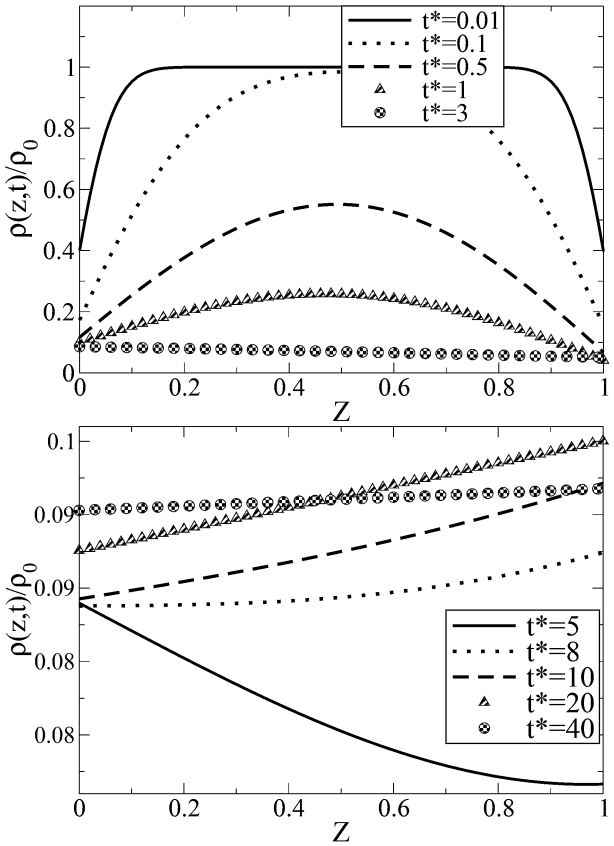

Fig. 5 Temporal behavior of $\rho(z, t)/\rho_0$ *vs.* $Z = z/d$ for several t^* when $S_0(s) = 1/\tau_0$ and $S_d(s) = 1/[(s + 1/\tau_a)\tau_d\tau_a]$. The curves represent the case where $\tau_D/\tau_0 = 5$, $\tau_d/\tau_0 = 1$, $\tau_{\kappa_d}/\tau_0 = \tau_{\kappa_0}/\tau_0 = 0.1$, and $\tau_\alpha/\tau_0 = 3.5$. Figure on the right represents short times, from $t^* = 0.01$ to $t^* = 3$ while the figure on the left shows $\rho(z, t)/\rho_0$ for longer times, from $t^* = 5$ to $t^* = 40$.

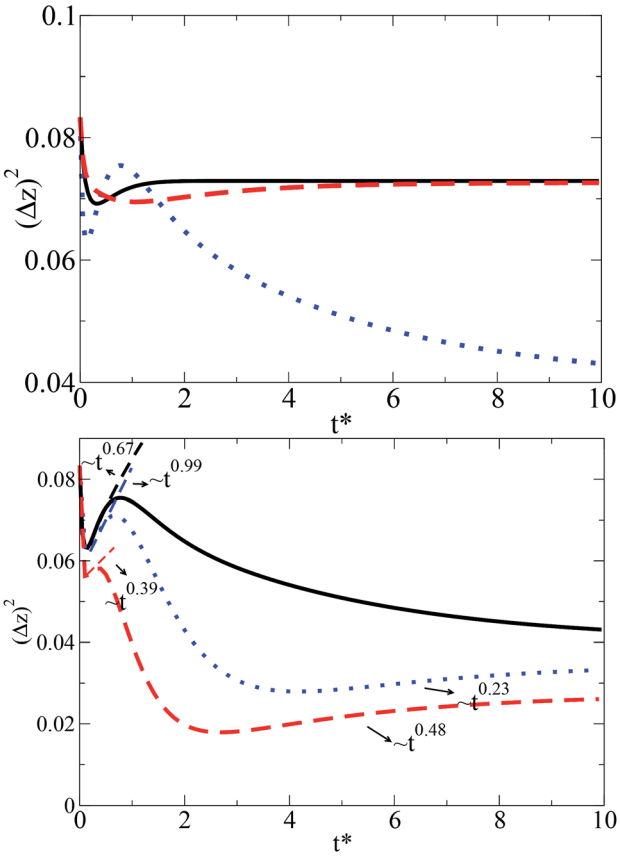

Fig. 6 $(\Delta z)^2$ *vs.* t^* *vs.* $t^* = 4t/\tau_D$ when $S_i(s) = 1/\tau_i$ (a) and $S_0(s) = 1/\tau_0$ and $S_d(s) = 1/[(s + 1/\tau_a)\tau_d\tau_a]$ (b). In (a), the solid line corresponds to $\tau_D/\tau_0 = 4$ and $\tau_d/\tau_0 = \tau_{\kappa_0}/\tau_0 = \tau_{\kappa_d}/\tau_0 = 1$. The dotted curve shows the case where $\tau_D/\tau_0 = 4$, $\tau_d/\tau_0 = \tau_{\kappa_d}/\tau_0 = 1$ and $\tau_{\kappa_0}/\tau_0 = 0.1$. The dashed line is the case where $\tau_D/\tau_0 = 40$, $\tau_{\kappa_0}/\tau_0 = \tau_{\kappa_d}/\tau_0 = 10$, and $\tau_d/\tau_0 = 20$. In (b), the solid line represents $\tau_D/\tau_0 = 4$, $\tau_d/\tau_0 = \tau_{\kappa_d}/\tau_0 = 1$, $\tau_{\kappa_0}/\tau_0 = 0.1$ and $\tau_a/\tau_0 = 1$. The dotted curve shows the case where $\tau_D/\tau_0 = 5$, $\tau_d/\tau_0 = 5$, $\tau_{\kappa_d}/\tau_0 = 1$, $\tau_{\kappa_0}/\tau_0 = 0.1$, and $\tau_a/\tau_0 = 3.5$. The dashed line represents the case where $\tau_D/\tau_0 = 5$, $\tau_d/\tau_0 = 1$, $\tau_{\kappa_d}/\tau_0 = \tau_{\kappa_0}/\tau_0 = 0.1$, and $\tau_a/\tau_0 = 3.5$.

$(\Delta z)^2/2t$), which changes with time. For the problem studied here, it is directly affected by the surfaces since immobilization by adsorption of the particles happens as they explore the media. Fig. 6a and b show $(\Delta z)^2$ *vs.* t^* employing the same parameters used in Fig. 2 and 4, respectively. In Fig. 6a, when $S_i(s) = 1/\tau_i$, the solid line corresponds to the case $S_0(t) = S_d(t)$. The curve decreases as expected since the distribution is shirking over time until it reaches a constant value. The dashed curve in Fig. 6a corresponds to the same parameters as in the dashed plot of Fig. 2. For long times, it reaches the same constant value as the solid line. This is governed by the adsorption times whose values are the same for both cases. Interestingly, for the dotted line (same parameters used for the dotted line in Fig. 2), $(\Delta z)^2$ takes a long time to reach a saturation point. There is an unbalance in the adsorption rates ($\tau_{\kappa_0} = \tau_{\kappa_d}/10$) which leads the bulk density of particles to evolute at a slower pace. Hence, the bulk particles take longer for complete immobilization compared to the other cases. Fig. 6b shows the cases $S_0(s) = 1/\tau_0$ and $S_d(s) = 1/[(s + 1/\tau_a)\tau_d\tau_a]$. The solid line is the same as the dotted line in Fig. 6a, since all the common parameters are the same and τ_a is small. The other two curves present long times to reach a constant value, even when $\tau_{\kappa_0} = \tau_{\kappa_d}$ (dashed), caused by the memory effect. It is worth pointing out that $(\Delta z)^2$ in certain cases decreases in the initial moments, then increases for a while until it finally starts decreasing to reach a constant value, as the three cases shown in Fig. 6b. In the period where $(\Delta z)^2$ increases, the distribution spreads, due to the desorption process from the surfaces. Therefore, we can find what kind of diffusive regime happens while the distribution broadens by looking at the exponent $(\Delta z)^2 \sim t^\alpha$, where α characterizes subdiffusion ($0 < \alpha < 1$) or superdiffusion ($\alpha > 1$).[20] In the three curves in Fig. 6b, all the exponents are smaller than 1, ranging from $\alpha = 0.23$ to $\alpha = 0.99$, behaving like subdiffusion induced by the surfaces.

In the spirit of the previous analysis, we show a log–log plot of $(\Delta z)^2$ *vs.* t^* for a set of parameters, chosen so the broadening time of the distribution is longer (obtained by scaling the parameters in the dashed curve in Fig. 6b by 10^{-5}). This figure shows how the adsorption process influences the spreading of the system and, consequently, leads to approximated subdiffusive regimes with $\alpha = 0.39$ and $\alpha = 0.48$ (regions where the

distribution is spreading). It is also interesting to note that this system is confined, in contrast to the case worked out in ref. 24. This feature is manifested in Fig. 7 by the two dashed lines, which is followed (for long times) by a stationary state. Furthermore, the shape of $(\Delta z)^2$ is different from the ones presented in ref. 24 in the sense that our system is initially considered to have $\rho(z, t = 0) = \rho_0$, which implies (for $t = 0$) in the greatest value of $(\Delta z)^2$. Therefore, as the system evolves, $(\Delta z)^2$ decreases due to adsorption and then increases due to spreading of the particles in the bulk until it reaches a stationary state. Note that it is usual to study anomalous diffusion in the literature by considering an infinity space, where the particle distribution is diffusing. Here, we establish a similar analysis, which can be performed only in the situations where the distribution is spreading out.

An interesting example of how the difference in the mechanism between the two surfaces affects the variance of the system is depicted in Fig. 8. For all the three plots, $\tau_D/\tau_0 = 4$, $\tau_d/\tau_0 = 1$. The solid line is calculated assuming that both surfaces are described by $S_i(s) = 1/\tau_i$, when $\tau_{\kappa_0} = \tau_{\kappa_d}/10$ (dotted curve in Fig. 2). The open circles represent the case in which the surface in $z = 0$ has chemisorption (delta function) and the surface at $z = d$ has physisorption (exponential function). In this case, $\tau_{\kappa_0} = \tau_{\kappa_d}/10$ and $\tau_a = \tau_{\kappa_d}/10$. As mentioned before, since τ_a is small, both set of parameters yield the same surface densities (dotted curves in Fig. 2 and circles in Fig. 4) and, as shown in Fig. 8, the same $(\Delta z)^2$. Therefore, the open circles in Fig. 8 represent the case for which the shortest adsorption time between the two surfaces is not the one for which the memory effect happens. Nevertheless, if we exchange the adsorption times by choosing $\tau_{\kappa_d} = \tau_{\kappa_0}/10$ (keeping the kernels unchanged), the $(\Delta z)^2$ obtained is the one shown by the dashed curve. Interestingly, when the surface densities are calculated, the behaviors of $\sigma_0(t)$ and $\sigma_d(t)$ replace each other, as shown by the inset in Fig. 8. The fact that the values of τ_{κ_d} and τ_{κ_0} are exchanged leading to an exchange between $\sigma_0(t)$ and $\sigma_d(t)$ is expected, since in the limit of small τ_α eqn (8) becomes the delta function representing chemisorption. What is not expected is the anomalous behavior shown in Fig. 8, where a combination

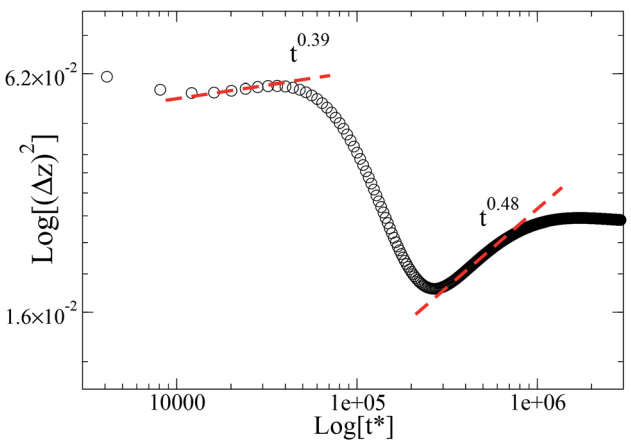

Fig. 7 $\log[(\Delta z)^2]$ *vs.* $\log[t^*$ *vs.* $t^* = 4t/\tau_D]$ for the scaled parameters of the dashed curve in Fig. 6.

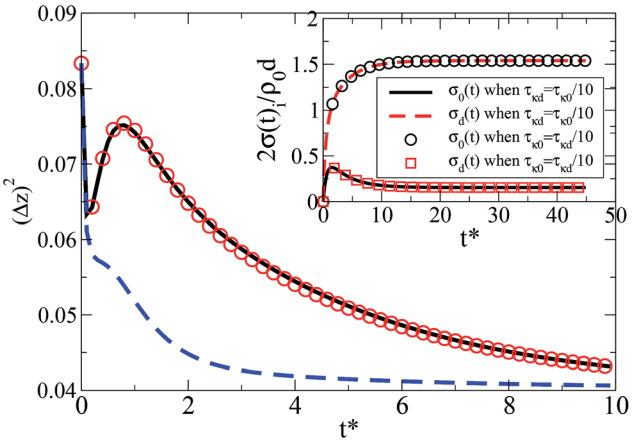

Fig. 8 $(\Delta z)^2$ *vs.* t^* *vs.* $t^* = 4t/\tau_D$. For all three plots, $\tau_D/\tau_0 = 4$, $\tau_d/\tau_0 = 1$. The solid line is calculated assuming that both surfaces are described by $S_i(s) = 1/\tau_i$, when $\tau_{\kappa_0} = \tau_{\kappa_d}/10$ (dotted curve in Fig. 2). The open circles represent the case where the surface in $z = 0$ has chemisorption (delta function) and the surface at $z = d$ has physisorption (exponential function). In this case, $\tau_{\kappa_d}/\tau_0 = 1$, $\tau_{\kappa_0}/\tau_0 = 0.1$ and $\tau_a/\tau_0 = 0.1$. The dashed curve is calculated for $\tau_{\kappa_0}/\tau_0 = 1$, $\tau_{\kappa_d}/\tau_0 = 0.1$ and $\tau_a/\tau_0 = 0.1$. The inset shows the surface densities associated with the open circles and dashed curves.

of the short adsorption time and memory effect changes the dynamics of the bulk particles. This indeed is an important result, never reported before, that may find application to systems in which particle separation of diffusion species is needed.

A system where the model presented here can be directly applied is in the surface control of dye adsorption, crucial in liquid crystal systems where photo-alignment is needed, such as for optical processing and storage. In these dye doped liquid crystal systems, the dyes may be adsorbed–desorbed whether there is light irradiation or not. The latter, called dark adsorption, is rather slow while adsorption in the presence of irradiation is a much faster phenomenon.[38] During irradiation, one substrate receives light while the other remains dark, thus, the dynamics of the two substrates are completely different. In ref. 39, this problem was theoretically explored by considering diffusing dyes in a potential field created near the surfaces by van-der-Waals and electrostatic interactions and the specific parameters of liquid crystals such as orientational and translational order parameters. It is found that, during irradiation of one surface, the kinetics of adsorbed dyes at one surface differs from the other. In fact, the results found in ref. 39 are similar to the ones shown in Fig. 2, which is indeed expected since it is assumed that the dyes bind to the substrate without memory effects, just as reported here for chemisorption, but in a simpler model. In fact, as mentioned before, the phenomenological parameters used here can be connected to microscopic parameters,[25] and a parallel with the model presented in ref. 39 can be established. Our model can also predict more complex behaviors since it takes into account memory effects as reported before.

Another interesting application for our model is the adsorption onto Janus grains.[40] These particles can be spherical, cylindrical or disk-like nanoparticles whose surfaces are treated to

present two or more physical–chemical properties. Recently, Carvalho *et al.* studied the adsorption of polyelectrolyte chains onto charged Janus nanospheres via Monte Carlo simulations.[41] The adsorption conditions were found to change when the particle size and screening length of the electrolyte varied. Furthermore, the behavior encountered differed from uniform spheres. Interestingly, the authors were able to find applications in biological systems such as for the complexation of non-homogeneously charged proteins. Our model incorporates the key ideas behind such phenomena. In fact, an extension of the current work is to solve the set of equations presented here in spherical coordinates to get analytical results of Janus spheres adsorbing neutral particles. A further extension is to consider the charged particles connecting the model with Poisson's equation.

The formalism presented above (and further developed in Appendix A) is important for several soft matter and chemical–physical systems since inhomogeneities, in general, are difficult to eliminate in experimental situations. In fact, there may be variation in adsorption energies for example resulting from different crystal planes, cracks, edges and lattice defects accessible by the diffusing particles.[42] Hopefully, the model presented here can be used in the mentioned applications and may inspire further developments in soft matter science and particles separation through non-identical adsorbing surfaces.

4. Concluding remarks

We have investigated theoretically a confined system of neutral particles that diffuse and may be adsorbed–desorbed by the limiting surfaces. It is considered that one of the surfaces present a different mechanism or dynamics than the other, a feature which is accounted for by using non-local kernels in the kinetic equations representing either chemisorption or physisorption. The surfaces and bulk densities as well as the variance of the system are analytically calculated. We find that even a small difference in the adsorption–desorption rate of one surface (relative to the other) can drastically affect the behavior of the whole system, including the variance, whose values show distinct behaviors depending on the choice of the characteristic times and memory effects. In particular, we demonstrate a very interesting phenomena characterized by the fact that the statistical comportment in the bulk presents an anomalous behavior and it is affected by the limiting surfaces, depending on the interchange of the parameters of the adsorption–desorption process. Knowing the behavior of such systems in a more realistic fashion, such as described here, is important in several applications such as separation by adsorption of diffusing species impedance characterization in dielectric media.

5. Appendix A: derivation of surface and bulk densities

We present the mathematical derivation of the model in more detail. We start from eqn (4) and (5). By replacing eqn (4) in (5), we get

$$G_0(s) = \frac{\kappa_0\left(B + \frac{\rho_0}{s}\right)}{S_0(s) + s}, \tag{10}$$

$$G_1(s) = \frac{\kappa_1\left(A(s)\,\sinh\left(d\sqrt{\frac{s}{D}}\right) + B(s)\,\cosh\left(d\sqrt{\frac{s}{D}}\right) + \frac{\rho_0}{s}\right)}{S_1(s) + s}. \tag{11}$$

The condition over the current implies that $D\mathrm{d}\rho(z,t)/\mathrm{d}z|_{z=0} = \mathrm{d}\sigma_0(t)/\mathrm{d}t$, or $D\mathrm{d}\rho(z,s)/\mathrm{d}z|_{z=0} = sG_0(s)$ (in Laplace's space), which allows us to write $A(s)$ in terms of $B(s)$. Then, $B(s)$ can be calculated by using the conservation of particles, $\sigma_0 + \sigma_d + \int_0^d \rho(z,t)\mathrm{d}z = \rho_0 d$. Once $A(s)$ and $B(s)$ are calculated, we can return to eqn (10) and (11) and write $G_0(s)$ and $G_1(s)$ as

$$G_0(s) = \frac{\kappa_0\rho\left(\kappa_1 s\left[\cosh\left(d\sqrt{\frac{s}{D}}\right) - 1\right] + D\sqrt{\frac{s}{D}}\alpha_1(s)\,\sinh\left(d\sqrt{\frac{s}{D}}\right)\right)}{sF(s)}, \tag{12}$$

and

$$G_1(s) = \frac{\kappa_1\rho_0\left(\kappa_0 s\left[\cosh\left(d\sqrt{\frac{s}{D}}\right) - 1\right] + D\sqrt{\frac{s}{D}}\alpha_0\,\sinh\left(d\sqrt{\frac{s}{D}}\right)\right)}{sF(s)}, \tag{13}$$

where

$$F(s) = \sqrt{\frac{s}{D}}\sinh\left(d\sqrt{\frac{s}{D}}\right)(D\alpha_0\alpha_1 + \kappa_0\kappa_1 s) + s\cosh\left(d\sqrt{\frac{s}{D}}\right)(\kappa_1\alpha_0 + \kappa_0, \alpha_1) \tag{14}$$

and $\alpha_0 = s + S_0(s)$ and $\alpha_1 = s + S_d(s)$. Now, in order to proceed and find the two surface densities, we need to calculate the inverse Laplace transform, which is possible only when the two kernels, $S_0(s)$ and $S_d(s)$ are known. The first case studied in this article corresponds to two surfaces presenting a chemisorption process, *i.e.*, $S_0(s) = 1/\tau_0$ and $S_d(s) = 1/\tau_d$. The inverse is calculated *via* Browinch's integral in the complex plane.[36] This integral is calculated by means of the residue theory, which depends only on the poles of the function. We note that eqn (12) and (13) have the same denominator, and therefore, the same poles, found by making the denominator equal to zero. By examination, one finds a pole in $s = 0$, while the others are found when

$$\sqrt{\frac{s}{D}}\sinh\left(d\sqrt{\frac{s}{D}}\right)(D\alpha_0\alpha_1 + \kappa_0\kappa_1 s) + s\cosh\left(d\sqrt{\frac{s}{D}}\right)(\kappa_1\alpha_0 + \kappa_0\alpha_1) = 0. \tag{15}$$

The roots of eqn (15) are found when we make $s = -\beta_n{}^2$ (n integer) and replace the kernels $S_0(s)$ and $S_d(s)$. In the first case studied here, where $S_0(s) = 1/\tau_0$ and $S_d(s) = 1/\tau_d$, we obtain

eqn (7) from (15), after making $\tau_D = d^2/D$, $\tau_{\kappa_i} = d/2\kappa_i$ and $d\beta_n/2\sqrt{D} = X_n$. If $S_0(s) = 1/\tau_0$ and $S_d(s) = 1/[(s + 1/\tau_a)\tau_d\tau_a]$, eqn (15) yields eqn (9). $G_0(t)$ and $G_d(t)$ are given as a sum of the residues in each pole. The residues in $s = 0$ and $s = -{\beta_n}^2$, are calculated by taking the following limits[36]

$$\mathrm{Res}(s=0) = \lim_{s\to 0} sG_i(s)\mathrm{e}^{ts} \tag{16}$$

$$\mathrm{Res}\left(s=-{\beta_n}^2\right) = \lim_{s\to -{\beta_n}^2}\left(s+{\beta_n}^2\right)G_i(s)\mathrm{e}^{ts},$$

where $i = 0$ or d and $n = 1, 2\ldots +\infty$. For the case where $S_0(s) = 1/\tau_0$ and $S_d(s) = 1/\tau_d$, by solving eqn (16), we get

$$\frac{2G_0(t)}{\rho_0 d} = \frac{2\tau_0\tau_{\kappa_d}}{\tau_d\tau_{\kappa_0} + (\tau_0 + 2\tau_{\kappa_0})\tau_{\kappa_d}} - \sum_n \frac{4\mathrm{e}^{\frac{-4{X_n}^2 t}{\tau_D}}\tau_0\tau_D\sin[X_n]\left[\left(4{X_n}^2\tau_d - \tau_D\right)\tau_{\kappa_d}\cos[X_n] + X_n\tau_d\tau_D\sin[X_n]\right]}{2X_n\Theta_1\cos[2X_n] + \Theta_2\sin[2X_n]}, \tag{17}$$

and

$$\frac{2G_d(t)}{\rho_0 d} = \frac{2\tau_d\tau_{\kappa_0}}{\tau_d\tau_{\kappa_0} + (\tau_0 + 2\tau_{\kappa_0})\tau_{\kappa_d}} - \sum_n \frac{4\mathrm{e}^{\frac{-4{X_n}^2 t}{\tau_D}}\tau_d\tau_D\sin[X_n]\left[\left(4{X_n}^2\tau_0 - \tau_D\right)\tau_{\kappa_0}\cos[X_n] + X_n\tau_0\tau_D\sin[X_n]\right]}{2X_n\Theta_1\cos[2X_n] + \Theta_2\sin[2X_n]}, \tag{18}$$

where

$$\Theta_1 = {\tau_D}^2(2\tau_0\tau_{\kappa_d} + 2\tau_d\tau_{\kappa_0} + \tau_{\kappa_0}\tau_{\kappa_d}) + 16\tau_0\tau_d\tau_{\kappa_0}\tau_{\kappa_d}{X_n}^4 - \tau_D{X_n}^2(\tau_0\tau_d(\tau_D + 12\tau_{\kappa_0}) + 4\tau_{\kappa_d}(\tau_{\kappa_0}(\tau_0 + \tau_d) + 3\tau_0\tau_d)), \tag{19}$$

and

$$\Theta_2 = 3{\tau_D}^2\tau_{\kappa_0}\tau_{\kappa_d} + 8\tau_0\tau_d{X_n}^4(\tau_D(\tau_{\kappa_0} + \tau_{\kappa_d}) + 14\tau_{\kappa_0}\tau_{\kappa_d}) - \tau_D{X_n}^2(\tau_0(5\tau_d\tau_D + 2\tau_D\tau_{\kappa_d} + 20\tau_{\kappa_0}\tau_{\kappa_d}) + 2\tau_d\tau_{\kappa_0}(\tau_D + 10\tau_{\kappa_d})). \tag{20}$$

When the kernel is changed (among the kernels studied here), the procedure for calculating the surface densities is the same since they result in first order poles.

The calculation of $\rho(z, t)$, and consequently $(\Delta z)^2$, follows a similar procedure. From eqn (4), and once $A(s)$ and $B(s)$ are known, one can write the following equation

Eqn (21) has a straightforward inversion. The first term $1/s$ has a simple Laplace inversion. The second term is a convolution of the function $1/\sqrt{s/D}$ and a function whose denominator is the same as in eqn (12) and (13), and therefore, the same procedure for calculating the inverse. The same applies to the third term of eqn (21). Just as for the surface densities, the calculation depends on the choice of the kernels, but it follows the procedures explained before. Nonetheless, after the inversion of eqn (21) we end up with two series summed, resulting in a long equation, and thus is not displayed here, manipulated with the software Mathematica 9.0.

Acknowledgements

The authors thank CNPq and Fundação Araucária for financial support.

References

1 J. L. de Paula, P. A. Santoro, R. S. Zola, E. K. Lenzi, L. R. Evangelista, F. Ciuchi, A. Mazzulla and N. Scaramuzza, *Phys. Rev. E: Stat., Nonlinear, Soft Matter Phys.*, 2012, **86**, 051705.
2 S. S. Andrews and D. Bray, *Phys. Biol.*, 2004, **1**, 137.
3 R. Erban and S. J. Chapman, *Phys. Biol.*, 2007, **4**, 16.
4 O. K. Dudko, A. M. Berezhkovskii and G. H. Weiss, *J. Phys. Chem. B*, 2005, **109**, 21296.
5 S. Wassen, R. Bordes, T. Geback, D. Bernin, E. Schuster, N. Lorenae and A.-M. Hermansson, *Soft Matter*, 2014, **10**, 8276.
6 S. Naumov, R. Valiullin, P. A. Monson and J. Karger, *Langmuir*, 2008, **24**, 6429.
7 H. V. Ribeiro, A. A. Tateish, L. G. A. Alves, R. S. Zola and E. K. Lenzi, *New J. Phys.*, 2014, **16**, 093050.
8 O. K. Dudko, A. M. Berezhkovskii and G. H. Weiss, *J. Phys. Chem. B*, 2005, **109**, 21296.
9 G. Barbero and L. R. Evangelista, *Adsorption Phenomena and Anchoring Energy in Nematic Liquid Crystals*, Taylor & Francis, London, 2006.
10 I. Janossy, *Phys. Rev. E: Stat. Phys., Plasmas, Fluids, Relat. Interdiscip. Top.*, 1994, **49**, 2957.
11 S. H. Perlmutter, D. Doroski and G. Moddel, *Appl. Phys. Lett.*, 1996, **69**, 1182.
12 M. Zhang, J. Soto-Rodriguez, I.-C. Chen and M. Akbulut, *Soft Matter*, 2013, **9**, 10155.

$$\frac{\rho(z,s)}{\rho_0} = \frac{1}{s} - \frac{\cosh\left[z\sqrt{\frac{s}{D}}\right]\left(\kappa_d\left(\alpha_0 + \kappa_0\sqrt{\frac{s}{D}}\sinh\left[d\sqrt{\frac{s}{D}}\right]\right) + \alpha_1\kappa_0\cosh\left[d\sqrt{\frac{s}{D}}\right]\right)}{\sqrt{\frac{s}{D}}F(s)} + \frac{\kappa_0\sinh\left[z\sqrt{\frac{s}{D}}\right]\left(\kappa_d s\left(\cosh\left[d\sqrt{\frac{s}{D}}\right] - 1\right) + \alpha_1 D\sqrt{\frac{s}{D}}\sinh\left[d\sqrt{\frac{s}{D}}\right]\right)}{sF(s)}. \tag{21}$$

13 M. Yaseen, H. J. Salacinski, A. M. Seifalian and J. R. Lu, *Biomed. Mater.*, 2008, **3**, 034123.
14 T. Ramanathan, A. A. Abdala, S. Stankovich, D. A. Dikin, M. Herrera-Alonso, R. D. Piner, D. H. Adamson, H. C. Schniepp, X. Chen, R. S. Ruoff, *et al.*, *Nat. Nanotechnol.*, 2008, **3**, 327.
15 R. Walder and D. K. Schwartz, *Soft Matter*, 2011, **7**, 7616.
16 R. D. Groot and S. D. Stoyanov, *Soft Matter*, 2010, **6**, 1682.
17 A. Nelson, D. Wang, K. Koynovb and L. Isa, *Soft Matter*, 2015, **11**, 118.
18 A. C. McUmber, P. S. Noonan and D. K. Schwartz, *Soft Matter*, 2012, **8**, 4335.
19 E. Beerdsen, B. Smit and D. Dubbeldam, *Phys. Rev. Lett.*, 2004, **93**, 248301.
20 R. Metzler, J.-H. Jeon, A. G. Cherstvya and E. Barkai, *Phys. Chem. Chem. Phys.*, 2014, **16**, 24128.
21 O. K. Dudko, A. M. Berezhkovskii and G. H. Weiss, *J. Chem. Phys.*, 2004, **121**, 11283.
22 L. Dagdug, A. M. Berezhkovskii, Y. A. Makhnovskii and V. Y. Zitserman, *J. Chem. Phys.*, 2007, **127**, 224712.
23 D. Ernst, J. Kohler and M. Weiss, *Phys. Chem. Chem. Phys.*, 2014, **16**, 7686.
24 S. K. Ghosh, A. G. Cherstvy and R. Metzler, *Phys. Chem. Chem. Phys.*, 2015, **17**, 1847–1858.
25 G. Barbero and L. R. Evangelista, *Phys. Rev. E: Stat., Nonlinear, Soft Matter Phys.*, 2004, **70**, 031605.
26 M. Levesque, O. Bénichou and B. Rotenberg, *J. Chem. Phys.*, 2013, **138**, 034107.
27 R. S. Zola, E. K. Lenzi, L. R. Evangelista and G. Barbero, *Phys. Rev. E: Stat., Nonlinear, Soft Matter Phys.*, 2007, **75**, 042601.
28 B. Lpez-Gonzlez, A. Dector, F. M. Cuevas-Muiz, N. Arjona, C. Cruz-Madridc, A. Arana-Cuencac, M. Guerra-Balczar, L. G. Arriaga and J. Ledesma-Garca, *Biosens. Bioelectron.*, 2014, **15**, 221.
29 A. Sparavigna, O. D. Lavrentovich and A. Strigazzi, *Phys. Rev. E: Stat. Phys., Plasmas, Fluids, Relat. Interdiscip. Top.*, 1994, **49**, 1344.
30 R. S. Zola, L. R. Evangelista, Y.-C. Yang and D.-K. Yang, *Phys. Rev. Lett.*, 2013, **110**, 057801.
31 P. Linse, *Soft Matter*, 2012, **8**, 5140.
32 B. Maximus, E. De Ley, A. De Meyere and H. Pauwels, *Ferroelectrics*, 1991, **121**, 103.
33 R. S. Zola, F. C. M. Freire, E. K. Lenzi, L. R. Evangelista and G. Barbero, *Chem. Phys. Lett.*, 2007, **438**, 144.
34 R. Hilfer, *Application of Fractional Calculus in Physics*, World Scientific, Singapore, 2000.
35 L. D. Landau and E. M. Lifshitz, *Electrodynamics of Continuous Media*, Pergamon Press, Oxford, 2nd edn, 1984.
36 M. P. Morse and H. Feshbach, *Methods of Theoretical Physics*, McGraw-Hill, New York, 1953.
37 H. Zhang and K. D'Have, *Mol. Cryst. Liq. Cryst.*, 2000, **27**, 351.
38 D. Voloschenko and O. D. Lavrentovich, *J. Appl. Phys.*, 1999, **86**, 4843.
39 O. V. Kuksenoka and S. V. Shiyanovskii, *Mol. Cryst. Liq. Cryst.*, 2001, **359**, 107.
40 P. G. de Gennes, *Rev. Mod. Phys.*, 1992, **64**, 645.
41 S. J. de Carvalho, R. Metzler and A. G. Cherstvy, *Phys. Chem. Chem. Phys.*, 2014, **16**, 15539.
42 A. W. Adamson and A. P. Gast, *Physical Chemistry of Surfaces*, Wiley, New York, 6th edn, 1997.

